

基于级联聚合物腔的光纤温度和磁场传感探头

李敏^{**}, 丛爱民^{*}, 曹万苍, 李晓伟

赤峰学院物理与智能制造工程学院, 内蒙古 赤峰 024000

摘要 设计了一个基于级联聚合物微腔的光纤传感探头, 实现了温度和磁场的同时传感探测, 有效克服了温度对磁场探测结果的影响。在单模光纤末端面依次蘸取磁性和非磁性聚合物薄膜, 并进行简单的紫外光固化即可制备该探头。所设计的探头制备过程简单, 成本低, 在航空航天、地球物理研究和医学等领域有着广泛的应用前景。

关键词 光纤光学; 光纤传感; 磁场强度; 温度; 聚合物

中图分类号 140.3040

文献标识码 A

DOI: 10.3788/CJL202249.0906004

1 引言

磁场的精确探测在航空航天、地球物理研究和医学领域有着重要的应用。多种类型的磁场传感器已用于探测环境中的磁场强度。其中, 光纤材料作为导光元件与磁性材料的结合被广泛应用于磁场传感器的制备中^[1-4], 该类传感器的灵敏度高, 可在恶劣环境中稳定工作, 具有远程传输的能力。近年来, 已报道了各式各样的基于磁流体材料的光纤传感器^[5-15]。该类型的光纤传感器具有灵敏度高、线性度好、结构紧凑等优良特性。然而, 当外加磁场增大到一定数值时, 分散在磁流体中的磁性粒子会发生团簇, 团簇导致磁流体的折射率突变^[16], 折射率的突变会对磁场传感器的特性产生很大的影响。为了避免磁流体的团簇现象对探测结果的影响, 用磁致伸缩材料代替磁流体材料与光纤结合制备传感结构, 磁致伸缩材料在强磁场下易发生形变, 对磁场具有较好的响应且不存在团簇现象^[17-19], 但其探测结果容易受环境温度的影响。为了避免温度对磁场测量结果的影响, 一种基于灵敏度矩阵方法的光纤磁场传感器被提出, 该传感器可同时监测温度和磁场, 虽然可以消除温度串扰, 且灵敏度较好, 但制备过程比较复杂^[20-21]。

本文设计了一种制备过程简单、可实现温度和

磁场同时测量的光纤传感探头。在单模光纤端面依次蘸取磁性和非磁性聚合物薄膜, 并利用紫外灯曝光固化即可制备该探头。级联的磁性和非磁性聚合物薄膜在光纤端面形成双法布里-珀罗干涉腔。通过在光刻胶中掺杂三氧化二铁纳米粒子可获得磁性聚合物薄膜, 经紫外光(UV)曝光后光刻胶将磁性纳米粒子包裹固化, 使得磁性聚合物薄膜具有一定磁性, 同时有效避免了强磁场作用下团簇现象的出现。在磁场的作用下, 只有磁性聚合物薄膜的折射率和腔长发生变化。温度变化时, 磁性和非磁性聚合物薄膜的折射率和腔长均发生改变, 从而使光谱中干涉峰的对比度和中心波长发生变化。实验监测了干涉谱中两个特征峰随温度和磁场的变化情况, 通过计算得到两个干涉峰的温度和灵敏度分别为 0 和 381.7 pm/°C, 磁场灵敏度分别为 48.9 pm/mT 和 55.4 pm/mT。根据实验结果, 利用传感矩阵便可实现磁场和温度的同时测量。该类传感器具有制作简单、成本低、能有效避免温度对磁场探测结果的影响, 在医疗、航空航天等领域将得到广泛应用。

2 制备过程和理论

采用简单蘸取和紫外灯曝光的方法制备级联聚合物微腔的光纤磁场传感探头。制备工艺如图 1 所

收稿日期: 2021-08-09; **修回日期:** 2021-10-16; **录用日期:** 2021-10-21

基金项目: 内蒙古自治区高等学校科研项目(NJZY19214)、内蒙古自治区大学生创新培训计划(S2021101380)、赤峰学院应用型示范课程建设项目(SFK20200904)、赤峰学院重点实验室建设项目(CFXYZD202007)、光电材料与原子核同位旋结构研究创新团队(cfykyextd202007)

通信作者: *c15026710904@163.com; **phdlimin@163.com

示。第一步,利用光纤切割工具将单模光纤端面切平,将切平的光纤端面向下垂直固定在三维电动平台上,并将切平的端面浸入到磁性聚合物薄材料中,磁性聚合物材料通过将磁性纳米粒子(四氧化三铁,粒径约为 10 nm)分散在光刻胶中并充分振荡获得,其质量分数为 5%。第二步,控制平台的移动速度为 100 m/s,向上提拉浸入在磁性聚合物材料中的光纤,将单模光纤从磁性材料中缓慢拉出,拉出后的光纤端面附着磁性聚合物薄膜。此时的聚合物膜依然为液态,为了避免蘸取第二层聚合物膜时两层膜发生流动混合,在蘸取第二层聚合物膜之前,将磁性聚合物膜放在紫外灯下曝光。磁性聚合物膜中的磁性纳米粒子对照射的光有一定的散射,为了使其充分固化,曝光时间设定为 20 s。第三步,曝光后磁性聚合物膜中出现一种酸,这种酸在一定温度下作为催化剂使光刻胶交联固化。这里,我们将曝光后的探头放在加热丝上烘烤固化,烘烤参数为在 65 °C 下烤 15 min,在 95 °C 下烤 45 min。固化的磁性聚合物膜在光纤末端形成微腔 I。微腔 I 在光纤纤芯处的最大厚度为 15 μm。

接下来,将集成了磁性聚合物微腔 I 的光纤继续浸入到聚合物溶液中,蘸取第二层非磁性聚合物薄膜,在光纤端面形成非磁性聚合物微腔 II,微腔 I 被微

腔 II 包裹,形成了一个级联的聚合物微腔结构。具体实验步骤和参数与制备磁性聚合物微腔 I 一致,如图 1(b) 所示。微腔 II 在光纤纤芯处的最大厚度为 40 μm。

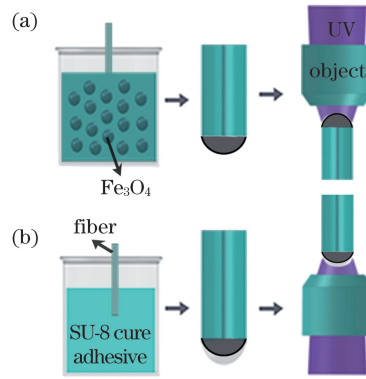


图 1 制备过程示意图。(a) 腔 I ;(b) 腔 II
Fig. 1 Schematic of preparation process. (a) Cavity I ; (b) cavity II

级联聚合物微腔光纤探头在光学显微镜下的照片如图 2(a) 所示。该级联聚合物微腔的最大厚度为 55 μm。将级联聚合物微腔光纤探头与宽带光源和光纤光谱仪连接,其反射干涉谱如图 2(b) 所示。可以看到,光纤探头的反射干涉谱具有较低的损耗,这说明本实验中配置的磁性聚合物膜具有较好的透光性,且级联聚合物双腔具有较规整的结构,这与我们在图 2(a) 中看到的吻合。

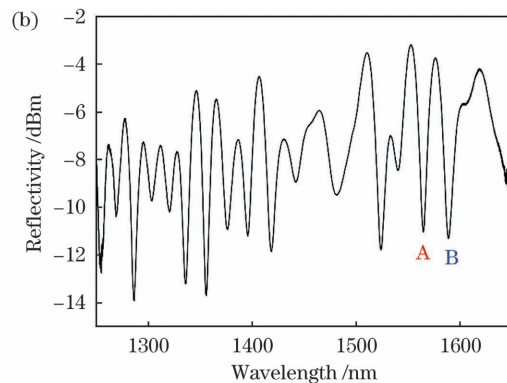
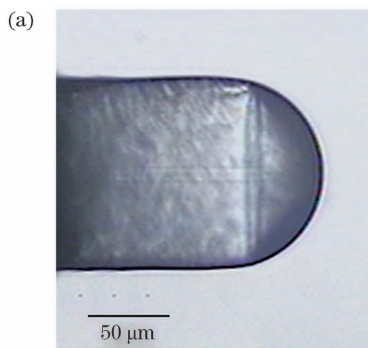


图 2 所设计的光纤传感探头的光学图片和干涉谱。(a) 光学图片 ;(b) 干涉谱

Fig. 2 Optical image and interferometric spectrum of proposed fiber sensing probe. (a) Optical image; (b) interferometric spectrum

入射光分别在光纤与磁性聚合物膜界面、磁性聚合物膜与非磁性聚合物界面、非磁性聚合物膜与空气界面处发生反射,三个面的反射光强分别用 I_1 、 I_2 和 I_3 表示,腔 I 和腔 II 的腔长分别为 L_1 和 L_2 ,折射率分别为 n_1 和 n_2 。在忽略高阶反射的情况下,该探头最终的反射光强 (I_{FP})^[15] 为

$$I_{FP} = I_1 + I_2 + I_3 - (I_1 I_2)^{1/2} \cos(4\pi n_1 L_1 / \lambda) - (I_2 I_3)^{1/2} \cos(4\pi n_2 L_2 / \lambda) + (I_1 I_3)^{1/2} \cos [4\pi(n_1 L_1 + n_2 L_2) / \lambda], \quad (1)$$

式中: λ 是入射光的波长。在没有磁场作用的情况下,磁性 SU-8 半球形聚合物薄膜中纳米粒子的磁矩方向是随机分布的,当传感探头置于磁场环境中时,分散在 SU-8 中的 Fe_3O_4 纳米颗粒被磁化,磁性纳米粒子的磁矩朝着磁场方向变化,从而磁性聚合物薄膜的折射率发生改变。同时,在外磁场的作用下,磁性聚合物薄膜发生形变,外磁场对法布里-珀罗(FP)干涉仪的腔长 L 有调制作用。因此,磁性聚合物薄膜的折射率和形状随着磁场强度的变化而改

变。由于磁性聚合物膜被非磁性聚合物膜包裹着,且聚合物材料的杨氏模量较小^[22],因此,磁性聚合物薄膜形状的改变同时引起非磁性聚合物膜的形状发生变化。根据式(1)可知,光纤探头反射光光强分布发生变化。此外,光纤探头置于温度变化的环境中时,非磁性和磁性聚合物膜的折射率和形状均发生变化,同样探头的光强分布也发生改变。

3 实验结果与讨论

首先我们研究该结构对温度的响应特性。可编程温控仪用来提供温度环境,光纤传感探头被固定在温控仪中的温控版上,通过温控仪的液晶显示屏设置温度变化范围为 25~50 °C。温度每变化 5 °C 记录一次反射干涉谱,分别记录 25, 30, 35, 40, 45, 50 °C 下的干涉谱,此时环境磁场恒定。我们选定图 2(b) 中的干涉峰 A 和干涉峰 B, 两个干涉峰随温度的变化如

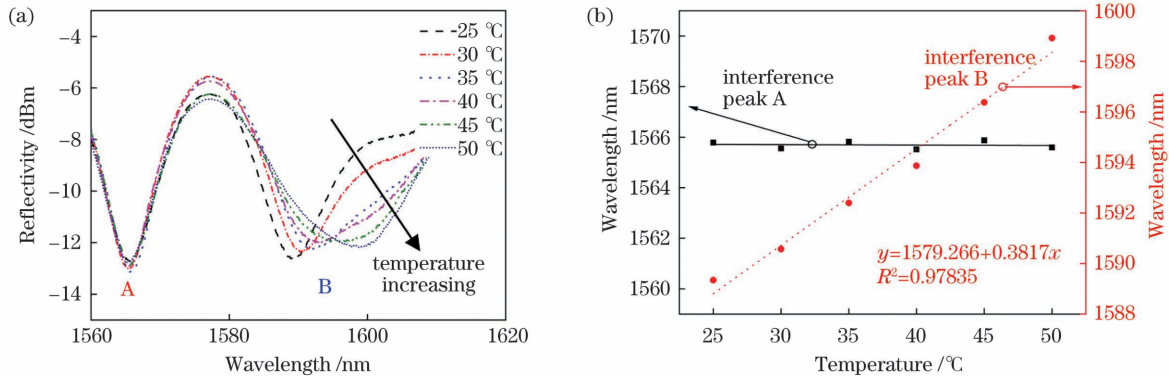


图 3 光纤传感探头对温度的响应。(a)不同温度下的干涉谱;(b)两个干涉峰的线性拟合结果

Fig. 3 Temperature response of fiber sensing probe. (a) Interference spectra at different temperatures; (b) linear fitting results of two interference peaks

当研究该光纤探头在磁场环境中的变化情况时,首先搭建了一个磁场强度特性的测试装置,如图 4 所示。光纤探头与高斯计的探头绑定在一起后固定在实验架上,并与永磁铁正对,高斯计用于记录光纤探头所处环境的磁场强度大小,磁场强度的大小显示

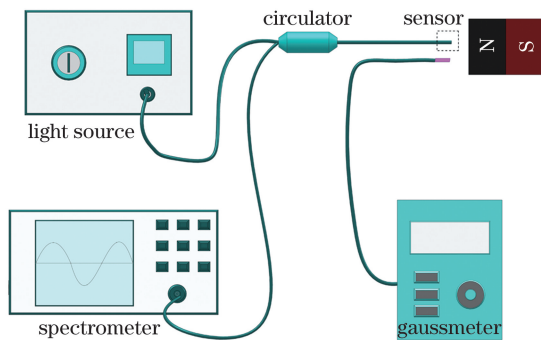


图 4 磁场探测装置

Fig. 4 Setup for magnetic field detection

图 3(a)所示,可以看到,随着温度的升高,干涉峰 A 几乎不发生变化,而干涉峰 B 的中心波长发生了明显的红移,从 1589.34 nm 移动到 1598.92 nm。干涉峰 A 由三个 FP 腔(磁性聚合物腔、非磁性聚合物腔、两个腔的混合腔)的干涉谱叠加形成,根据三个腔的腔长尺寸可知,在测量光谱范围内,混合腔的干涉峰最密,其次是非磁性聚合物腔,磁性聚合物腔的干涉峰最稀疏。温度升高时,三个腔的腔长都变大,干涉峰同时向长波长方向移动,非磁性聚合物腔的干涉峰移动速度与混合腔干涉峰的接近,当这两个腔的干涉峰波谷刚好出现在磁性聚合物腔干涉峰波峰比较平坦的位置处时,随着温度的升高,此位置处叠加的干涉峰几乎不发生移动。记录两个干涉峰在每个温度记录点处的中心波长,如图 3(b)所示,其中 R^2 为模型的拟合度。对这些记录点进行线性拟合,得到两个干涉峰的温度灵敏度分别为 0 和 381.7 pm/°C。

在高斯计的液晶显示屏上。

调整磁铁与光纤探头的相对位置,改变探头所处环境的磁场强度大小,磁场强度的变化引起腔 I 的折射率和腔长同时发生改变,磁性聚合物薄膜的折射率随着磁场强度的增加而逐渐增大^[16],且磁铁与传感探头正对,所以腔长随着磁场强度的增加而变大,最终腔 I 对应的干涉峰向长波长方向移动。从图 5(a)中可以看到,当磁场强度从 0 增大到 50 mT 时,磁场引起腔 I 特征峰发生了一定的红移,由于腔 I 被腔 II 包裹着,而腔 II 对磁场不敏感,因此当环境磁场强度增大时,腔 II 限制了腔 I 的膨胀。但由于聚合物材料的杨氏模量较小,因此腔 I 的形变引起腔 II 的形状改变,腔 II 的折射率和腔长得到调制。最终腔 II 的特征峰也向着长波长方向移动。干涉峰 A 从 1564.691 nm 移动到了 1567.139 nm,干涉峰 B 从 1588.862 nm 移动到了 1591.716 nm。

记录每个磁场强度处干涉峰 A 和 B 的中心波长, 并对其进行线性拟合, 得到干涉峰 A 和 B 的磁场灵敏度

度分别为 48.9 pm/mT 和 55.4 pm/mT, 线性度分别达到了 0.95242 和 0.96132。

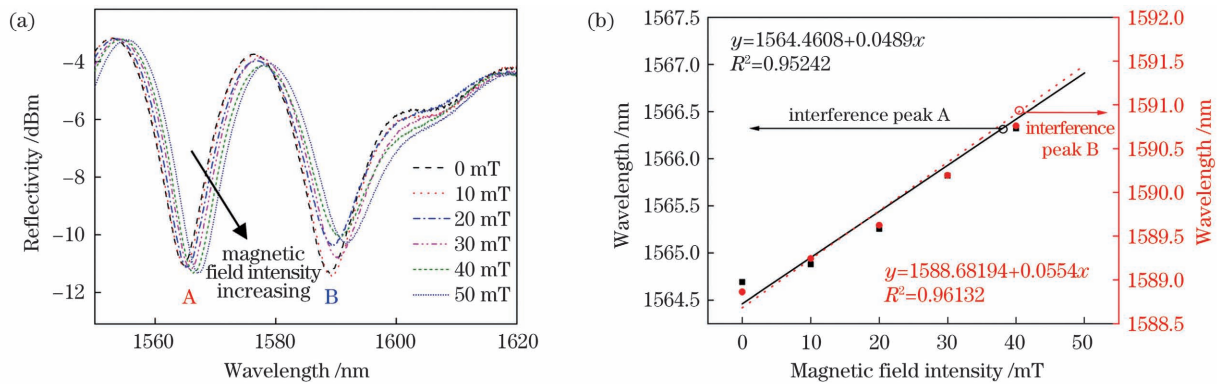


图 5 光纤传感探头对磁场的响应。(a)干涉谱;(b)两个干涉峰的线性拟合结果

Fig. 5 Response of fiber sensing probe to magnetic field. (a) Interference spectra; (b) linear fitting results of two interference peaks

当环境温度和磁场改变时,图 3(a)和 5(a) 中干涉峰的中心波长位置发生变化,监测两个干涉峰对温度和磁场的响应,级联聚合物微腔光纤探头在用于温度和磁场同时测量时可以用过以下矩阵实现:

$$\begin{bmatrix} \Delta\lambda_A \\ \Delta\lambda_B \end{bmatrix} = \begin{bmatrix} S_{MA} & S_{TA} \\ S_{MB} & S_{TB} \end{bmatrix} \begin{bmatrix} \Delta M \\ \Delta T \end{bmatrix}, \quad (2)$$

式中: ΔM 和 ΔT 分别代表环境中磁场和温度的变化量,环境中磁场的变化通过高斯计测量,温度变化通过温控仪测量; $\Delta\lambda_A$ 和 $\Delta\lambda_B$ 分别为温度和磁场变化引起的干涉峰 A 和 B 的波长漂移,单位为 pm; S_{MA} 和 S_{TA} 分别为干涉峰 A 的磁场和温度灵敏度,本文中 S_{MA} 为 48.9 pm/mT, S_{TA} 为 0; S_{MB} 和 S_{TB} 分别为干涉峰 B 的磁场和温度灵敏度,本文中 S_{MB} 为 55.4 pm/mT, S_{TB} 为 381.7 pm/°C。

4 结 论

采用简单的紫外灯曝光法,在单模光纤端面制备了级联的磁性和非磁性聚合物薄膜,实现了温度和磁场的同时传感,有效避免了温度对传统磁场传感器磁场测量结果的影响,光纤传感探头干涉谱中 1565 nm 和 1590 nm 附近两个干涉峰的磁场强度灵敏度分别达到了 48.9 pm/mT 和 55.4 pm/mT,温度灵敏度分别为 0 和 381.7 pm/°C。

参 考 文 献

[1] Chen L X, Huang X G, Zhu J H, et al. Fiber magnetic-field sensor based on nanoparticle magnetic fluid and Fresnel reflection[J]. Optics Letters, 2011, 36(15): 2761-2763.

[2] Luo L F, Pu S L, Dong S H, et al. Fiber-optic magnetic field sensor using magnetic fluid as the cladding [J]. Sensors and Actuators A: Physical, 2015, 236: 67-72.

[3] Zhang J Y, Qiao X G, Yang H Z, et al. All-fiber magnetic field sensor based on tapered thin-core fiber and magnetic fluid[J]. Applied Optics, 2017, 56(2): 200-204.

[4] Sun B, Fang F, Zhang Z, et al. High-sensitivity and low-temperature magnetic field sensor based on tapered two-mode fiber interference [J]. Optics Letters, 2018, 43(6): 1311-1314.

[5] Zheng J, Dong X Y, Zu P, et al. Intensity-modulated magnetic field sensor based on magnetic fluid and optical fiber gratings [J]. Applied Physics Letters, 2013, 103(18): 183511.

[6] Dai J X, Yang M H, Li X B, et al. Magnetic field sensor based on magnetic fluid clad etched fiber Bragg grating[J]. Optical Fiber Technology, 2011, 17(3): 210-213.

[7] Zheng J, Dong X Y, Zu P, et al. Magnetic field sensor using tilted fiber grating interacting with magnetic fluid[J]. Optics Express, 2013, 21(15): 17863-17868.

[8] Gao L, Zhu T, Deng M, et al. Long-period fiber grating within D-shaped fiber using magnetic fluid for magnetic-field detection[J]. IEEE Photonics Journal, 2012, 4(6): 2095-2104.

[9] Gao R, Jiang Y, Abdelaziz S. All-fiber magnetic field sensors based on magnetic fluid-filled photonic crystal fibers[J]. Optics Letters, 2013, 38(9): 1539-1541.

[10] Zu P, Chan C C, Lew W S, et al. Temperature-insensitive magnetic field sensor based on nanoparticle magnetic fluid and photonic crystal fiber [J]. IEEE

- Photonics Journal, 2012, 4(2): 491-498.
- [11] Ji D Y, Ruan S C, Liu T G, et al. All-fiber-optic vector magnetometer based on nano-magnetic fluids filled double-clad photonic crystal fiber[J]. Sensors and Actuators B: Chemical, 2017, 238: 518-524.
- [12] Miao Y P, Wu J X, Lin W, et al. Magnetic field tunability of optical microfiber taper integrated with ferrofluid[J]. Optics Express, 2013, 21(24): 29914-29920.
- [13] Zheng Y Z, Dong X Y, Chan C C, et al. Optical fiber magnetic field sensor based on magnetic fluid and microfiber mode interferometer [J]. Optics Communications, 2015, 336: 5-8.
- [14] Luo L F, Pu S L, Tang J L, et al. Reflective all-fiber magnetic field sensor based on microfiber and magnetic fluid[J]. Optics Express, 2015, 23(14): 18133-18142.
- [15] Chen Y F, Han Q, Liu T G, et al. Optical fiber magnetic field sensor based on single-mode-multimode-single-mode structure and magnetic fluid [J]. Optics Letters, 2013, 38(20): 3999-4001.
- [16] Yang S Y, Chen Y F, Horng H E, et al. Magnetically-modulated refractive index of magnetic fluid films [J]. Applied Physics Letters, 2002, 81(26): 4931-4933.
- [17] Yang M H, Dai J X, Zhou C M, et al. Optical fiber magnetic field sensors with TbDyFe magnetostrictive thin films as sensing materials [J]. Optics Express, 2009, 17(23): 20777-20782.
- [18] Dai Y T, Yang M H, Xu G, et al. Magnetic field sensor based on fiber Bragg grating with a spiral microgroove ablated by femtosecond laser[J]. Optics Express, 2013, 21(14): 17386-17391.
- [19] Rao C N, Nakate U T, Choudhary R J, et al. Defect-induced magneto-optic properties of MgO nanoparticles realized as optical-fiber-based low-field magnetic sensor[J]. Applied Physics Letters, 2013, 103(15): 151107.
- [20] Zhao Z Y, Tang M, Gao F, et al. Temperature compensated magnetic field sensing using dual S-bend structured optical fiber modal interferometer cascaded with fiber Bragg grating [J]. Optics Express, 2014, 22(22): 27515-27523.
- [21] Kang S X, Zhang H, Liu B, et al. A fiber-optic interferometer based on non-adiabatic fiber taper and long-period fiber grating for simultaneous measurement of magnetic field and temperature [J]. Journal of Optics, 2016, 18(1): 015802.
- [22] Larsen T, Keller S, Schmid S, et al. Fabrication and characterization of SRN/SU-8 bimorph cantilevers for temperature sensing [J]. Microelectronic Engineering, 2011, 88(8): 2311-2313.

Temperature and Magnetic Field Fiber Sensing Probe Based on Cascaded Polymer Cavities

Li Min^{*,}, Cong Aimin^{*}, Cao Wancang, Li Xiaowei

College of Physics and Intelligent Manufacturing Engineering, Chifeng College, Chifeng 024000, Nei Monggol, China

Abstract

Objective A compact fiber sensing probe based on cascaded polymer microcavities is proposed in this paper for measuring magnetic field and temperature. This fiber probe effectively overcomes the influence of temperature on the detection results of magnetic field. There are broad applications in the fields of aerospace, geophysical research, and medicine.

Methods The proposed fiber sensor based on cascaded Fabry-Perot(FP) cavities is fabricated using the method of dipping and ultraviolet(UV) curing. The schematic of fabrication process is shown in Fig. 1. First, the magnetic SU-8 photoresist is achieved by doping 5% mass fraction Fe_3O_4 nanoparticles into the SU-8 photoresist and then it is ultrasonic vibrated with an ultrasonic agitator at 40 kHz for 2 h. The Fe_3O_4 nanoparticles can be homogeneously dispersed in the SU-8 photoresist, and the nanoparticle diameter is only around 10 nm. The magnetic SU-8 photoresist has a good transmittance to infrared light. The end-face of single-mode fiber (SMF) is cut flat and dipped into the magnetic SU-8 photoresist. A perfect elliptical polymer film on the end surface of SMF is achieved after the optical fiber is pulled out, which is combined with SMF to form an FP cavity (cavity I). The maximum thickness of the cavity I is 15 μm . The cavity I is soft baked on a hot plate at 65 $^\circ\text{C}$ for 15 min and 95 $^\circ\text{C}$ for 2 h, and the UV source is focused on the fiber tip. The exposure dose and exposure time of the UV source are 400 mJ/cm^2 and 15 s,

respectively. Second, the FP cavity in the first step is dipped into the SU-8 photoresist and the polymer thin films (cavity II) are integrated with the cavity I after the optical fiber is pulled out. The cavity II is baked and cured using the same experimental steps and under the same conditions as those of the first step. Eventually, the fiber sensor based on cascaded FP cavities is obtained [Fig. 1(b)].

Results and Discussions When the temperature increases from 25 °C to 55 °C at a constant magnetic fields, the dip A and dip B shift to the longer wavelength [Fig. 3(a)]. The central wavelength of the dip A barely moves, and the dip B shifts from 1589.34 nm to 1598.92 nm. The shift of interference peak at each temperature measurement point is measured. Three heat-up and cooling experiments are done. The mean wavelength shift and error bars of the measurement at each temperature point are calculated and fitted linearly. The temperature sensitivities of dips A and B are 0 and 381.7 pm/°C, respectively [Fig. 3(b)]. One can find that the fiber cantilever taper for sensing temperature is with an excellent linear relationship and good repeatability.

When the fiber tip is placed in the magnetic field environment, the reflectance spectrum at each magnetic field intensity is recorded by the spectrometer [Fig. 5(a)]. The dips A and B are used to record these details. When the magnetic field varies from 0 to 50 mT with 10 mT as a step, the dip A shifts from 1564.691 nm to 1567.139 nm and the dip B shifts from 1588.862 nm to 1591.716 nm, respectively. The experimental results show that the spectrum moves towards the long-wavelength direction with the increase of magnetic field. The experimental results agree well with the theoretical ones. Three repeated experiments are done, and the mean value of the center wavelength of the interference peak and the measurement error at each magnetic field are calculated. The linear fitting of the center wavelength positions of the dips A and B shows that the magnetic field intensity sensitivities of the sensing probe reach 48.9 pm/mT and 55.4 pm/mT, and the linearities are 0.95242 and 0.96132, respectively [Fig. 5(b)].

Conclusions A compact fiber sensing probe is proposed, and the magnetic field and temperature are simultaneously measured. The cascaded magnetic and non-magnetic polymer films are integrated with the fiber to form the sensing probe, which is obtained using simple dipping and UV curing technologies. The temperature sensitivities of dips A and B are 0 and 381.7 pm/°C, and the magnetic fields sensitivities are 48.9 pm/mT and 55.4 pm/mT, respectively. The simultaneous measurements of magnetic field and temperature are obtained using the method of sensitivity matrix. The sensing probe may find a widespread application in aerospace space, geophysical research, and medical fields due to its easy fabrication process, high sensitivity, compactness, and good stability.

Key words fiber optics; fiber sensing; magnetic field intensity; temperature; polymer